Accelerated Degradation Testing and Failure Mechanism Analysis of Metallized Film Capacitors for AC Filtering

Bo Yao, *Graduate Student Member, IEEE*, Xing Wei, *Graduate Student Member, IEEE*, Yichi Zhang, *Graduate Student Member, IEEE*, Pedro Correia, Rui Wu, *Senior Member, IEEE*, Sungyoung Song, Ionut Trintis, *Member, IEEE*, Haoran Wang, *Member, IEEE*, and Huai Wang, *Senior Member, IEEE*

***Abstract*—Film capacitors for ac filtering play a crucial role in various industrial applications, such as wind power and traction systems. However, current research lacks studies on the aging and failure analyses of high-power ac film capacitors subjected to realistic stresses. This article addresses this gap by presenting degradation testing and failure analysis of metallized film capacitors employed in megawatt (MW) power converters for ac filtering purposes. First, accelerated aging tests are performed on ac filter capacitors based on realistic stresses for more than 3500 h. Testing results on electrothermal parameters are recorded, and derivative models of parameter aging are obtained. The analysis reveals that electrochemical corrosion is the primary aging factor, with negligible capacitance reduction until catastrophic failure occurs. Further investigation, including temperature rise results and microstructure evaluation, indicates that the melting of the dielectric film is a crucial precursor to catastrophic failure. Finally, the possible degradation and failure mechanisms for this type of ac filtering capacitors are summarized. The observations provide a new perspective on the possible failure mechanisms and condition monitoring of film capacitors in ac filtering applications.**

***Index Terms*—AC filtering, accelerated aging, electrothermal parameter, failure mechanisms, metallized film capacitors.**

I. Introduction

METALLIZED film capacitors are widely used in power electronic converters applications with high voltage and high current [1]. AC filtering film capacitors play a crucial role in industrial applications, such as wind power and traction systems [2] and [3]. The degradation of metallized film capacitors poses a significant concern, as it can compromise the filtering capability and potentially lead to severe catastrophic accidents in operational systems [4]. Therefore, it is significant for industrial applications to understand the degradation and failure mechanism of ac filtering film capacitors is of paramount importance for ensuring safety and reliability.

Even though metallized film capacitors have the capabilities with high reliability, low losses, and self-healing, they still degrade and fail because of overstresses or long-term degradation cumulation [5], [6]. The failure factors of the metallized film capacitors mainly can be divided into the dielectric breakdown and electrode corrosion [7]. The failure factors of metallized film capacitors primarily fall into two categories: 1) dielectric breakdown and 2) electrode corrosion [7]. Electrode corrosion can be further classified into atmospheric corrosion, which does not necessitate voltage stress, and electrochemical corrosion, which requires the involvement of ac voltage [8].

Accelerated testing is a significant method to investigate the degradation and mechanism of power electronics [9]. In [10] and [11], the dc voltage and temperature are employed as accelerated aging stress factors for metallized film capacitors. Under high dc voltage test conditions, defects within the dielectric material can instigate localized breakdowns in the dielectric film, resulting in a reduction in the capacitance value of the capacitor. Meanwhile, for impulse discharge applications, the primary cause of film capacitor failure lies in the capacitance loss due to partial discharges [12]. The research in [13] reveals that humidity corrosion can significantly impact the failure of metallized film capacitors, with the corrosion occurring independently of electrical stress. In electromagnetic interference (EMI) suppression applications, it is found that interlayer air causes a large number of electrochemical corrosion spots in ac metallized film capacitors [14]. Corrosion emerges as the primary failure mechanism for EMI ac capacitors, with severe corrosion observed near the edge of the electrode [15]. Electrodes undergoing oxidation due to electrochemical corrosion

Manuscript received 12 September 2023; revised 9 December 2023; accepted 22 January 2024. Date of publication 30 January 2024; date of current version 20 March 2024. Recommended for publication by Associate Editor Ke (SSGAE | OJ GAE | GE) Ma. *(Corresponding author: Xing Wei.)*

Bo Yao, Xing Wei, Yichi Zhang, and Huai Wang are with the Department of Energy Technology, Aalborg University, 9220 Aalborg, Denmark (e-mail: ybo@energy.aau.dk; xwe@energy.aau.dk; yzhang@energy.aau.dk; hwa@energy.aau.dk).

Pedro Correia, Rui Wu, and Sungyoung Song are with the Vestas Wind Systems A/S, 9220 Aalborg, Denmark (e-mail: paabc@vestas.com; RIWUB@vestas.com; suysn@vestas.com).

Ionut Trintis is with the Siemens Gamesa Renewable Energy, 7330 Brande, Denmark (e-mail: iotri@vestas.com).

Haoran Wang is with the Three Gorges Intelligent Industrial Control Technology Corporation, Ltd., Wuhan 430070, China (e-mail: wang_haoran@ctg.com.cn).

Color versions of one or more figures in this article are available at https://doi.org/10.1109/TPEL.2024.3360373.

Digital Object Identifier 10.1109/TPEL.2024.3360373

TABLE I
TEST PARAMETERS AND FAILURE ANALYSIS OF METALLIZED FILM CAPACITORS FOR AC FILTERING IN THE EXISTING LITERATURE

Aging Testing Parameters for Metallized Film AC Capacitor				Applicable field	Main failure phenomenon or mechanism obtained	Ref.
AC voltage	AC current	Capacitance	Test frequency			
305 V	< 1 A	0.33 μF	not given	EMI suppression	Weight of the failed capacitor increases, and the plastic package cannot prevent water intrusion	[8]
300 V	< 1 A	not given	50 Hz	EMI suppression	Interlayer air causes a large amount of electrochemical corrosion spots	[14]
330/363 V	0.23 A	2.2 μF	50 Hz	EMI suppression	Corrosion is the main failure mechanism, and the corrosion is severe near the edge of the electrode	[15]
270 V	0.039 A	0.47 μF	50 Hz	EMI suppression	Under the effect of electrochemical corrosion, the capacitance decreases and ESR increases.	[16]
305 V	0.045 A	0.47 μF	50 Hz	EMI suppression	Positive correlation between electrode corrosion and temperature / humidity at AC voltage	[17]
100 V	0.2 A	8 μF	50Hz−1 kHz	Low-power motor system	For excessive current density caused by heating may be the main cause of failure	[18]
230 V	0.016 A	0.22 μF	50 Hz	Low-power sources and chargers	Film X2 capacitors are susceptible to electro-chemical corrosion	[19]
200V–310 V	< 1 A	0.001−1μF	not given	EMC-filters	Some of the failed samples showed the decrease in capacitance and some do not.	[20]
275 V	< 1 A	0.1 μF	not given	EMI suppression	Capacitance change of the samples caused by heat aging is low	[21]
200V–600 V	< 1 A	not given	60 Hz	Low-power converter system	Electrochemical corrosion generally occurs at AC voltages in excess of 250 Vac	[22]
>500 V	>10 A	>10 μF	AC fundamental frequency	AC Filtering for high- power converters	Unknown	Lack

induced by ac voltage in high-temperature and high-humidity environments are discussed in [16] and [17]. Brown [18] indicated that excessive current density resulting from heating may be the principal cause of failure for low-power ac film capacitors. In low-power supply and charging applications, film X2 capacitors are similarly susceptible to electrochemical corrosion [19]. In [20], the metallized film layer is almost completely degraded in the failed capacitor in high-temperature and high-humidity aging tests, while no significant changes are found in the dielectric film layer. In aging testing involving ac voltage at high temperature and medium humidity [21], the total electrode area exhibits a negligible change, and the capacitance decreases only slightly. Nevertheless, under the influence of galvanic corrosion, the resistance of the metal layer of the capacitor electrode increases. In addition, different voltage testing reveals that electrochemical corrosion generally occurs at ac voltages over 250 Vac [22].

The test parameters, application fields, and failure mechanisms of metallized film capacitors for ac filtering in the existing literature are summarized in Table I. The existing accelerated aging tests and failure mechanism analyses of ac film capacitors are mainly applied in EMI suppression [23] and low-power converter filtering [24], with low current levels and low capacitance values.

Existing studies are still lacking in aging and failure analyses of high-power ac film capacitors under realistic stresses (ac voltage $>$ 500 V, ac current $>$10 A, and capacitance $>$ 10 μF). However, existing studies cannot be easily extended to other types and applications of capacitors because the failure mechanism is affected by their specific design structure and stress conditions. It is necessary to perform further degradation testing and failure mechanism analysis of high-power metallized film capacitors for ac filtering with realistic stresses.

This article aims to investigate the aging impact factors and the respective failure mechanisms of a type of ac power filtering film capacitors used for megawatt (MW) power converters. Based on the analysis of failure modes, calculation of aging indicators, and about 3500 h of accelerated aging test testing, a type of degradation and failure mechanism is summarized. This is demonstrated as follows.

1) The capacitance has negligible change under the specific testing conditions of the applied testing samples until the testing samples catastrophically fail.
2) The degradation process is accompanied by a significant increase in the hot spot temperature. Finally, the capacitor catastrophically failed due to the melting of the dielectric films.
3) With the capacitor aging, the equivalent series resistance (ESR) gradually increases, which causes the hot spot temperature to rise. The parallel insulation resistance decreases in the high-temperature stage, thus causing the hot spot temperature to rise significantly at this stage.

The rest of this article is organized as follows. Section II presents the possibility of aging and failure factors. Section III presents experiment configuration and testing results. Section IV gives the degradation indicators extraction. Aging and failure analyses based on test results are shown in Section V. Microverification and failure mechanism summary are given in Section VI. Finally, Section VII concludes this article.

II. METALLIZED FILM CAPACITOR STRUCTURE AND POSSIBLE FAILURE MODES

A. Physical Structure and Equivalent Electrical Model

The equivalent electrical model of metallized film ac capacitors is given in Fig. 1(a). A single Delta − connection ac capacitor is composed of three metallized film capacitor units and the three terminals [25]. In a single capacitor unit, r_{end}, r_m, r_P, and C represent terminal parasitic resistance, ESR, equivalent parallel insulation resistance, and capacitance, respectively [26], [27].

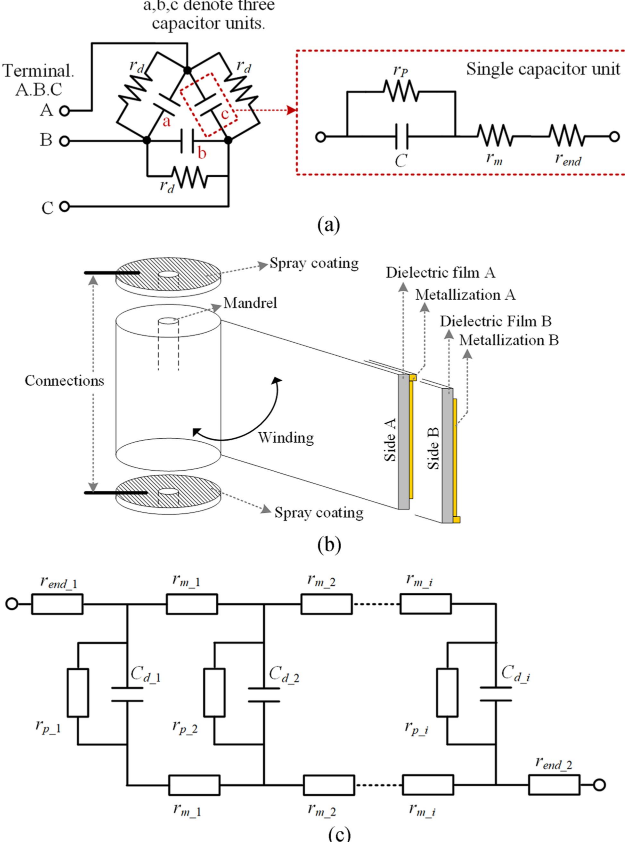

Fig. 1. Equivalent electrical model and general structure of metallized film ac capacitors. (a) Equivalent electrical model of AC metallized film capacitors. (b) Physical structure of single capacitor unit in AC metallized film capacitors. (c) Equivalent electrical model of single capacitor unit.

The parasitic inductance of the capacitor typically falls within the range of tens of nanohenries, which is insignificant compared with the equivalent resistance. [24]. In addition, each capacitor unit is connected in parallel with a discharge resistor r_d.

The structure of a metallized film capacitor unit is shown in Fig. 1(b) [28]. In each unit, two dielectric film layers are wound around an insulated cylindrical mandrel. The thickness of the metallized layer (the metallization A and the metallization B) evaporated onto the film is of the order of nanometers. The thickness of the polypropylene dielectric layer (the dielectric film A and dielectric film B) is of the order of micrometers [18], [29].

The equivalent electrical model of the metallized film capacitor unit is shown in Fig. 1(c). The film layers can be divided into i parts area in parallel, where each part can be considered as a capacitor submodule [30]. In this submodule, r_{m_i}, r_{P_i}, and C_{d_i} represent ESR, equivalent parallel insulation resistance, and capacitance in ith capacitor module, respectively.

B. Possible Failure Modes for Metallized Film Capacitors

According to the description in Section I, metallized film capacitors have three possible failure modes, which are dielectric breakdown, humidity corrosion, and electrochemical corrosion [7], [8]. This section analyzes the failure principle, the change of the corresponding equivalent circuit, and the characterization of the failure parameters for those three failure modes, as given in Fig. 2.

1) Dielectric Breakdown: When metallized film capacitors are operated near the rated voltage, the voltage spikes can cause local breakdown of the dielectric films, which results in long-term capacitive degradation of the capacitor [8]. From the partial film structure of dielectric breakdown in Fig. 2, the part of the dielectric film layer is broken through, accompanied by the disconnection of the metallized film layer in the same region [11].

In correspondence with the equivalent circuit, the dielectric film and the metallized film are modeled as individual submodules denoted by i connected in parallel. The dielectric breakdown can be described as the failure of the circuit structure related to the dielectric film, such as the failure of C_{d_1} and r_{p_1} in the dielectric breakdown part of Fig. 2. As the number of such breakdown points increases, the capacitance gradually decreases until reaching a critical point where the capacitor ultimately fails [31].

2) Humidity Corrosion: Failure of metallized film capacitors can be affected by humidity corrosion. Moisture penetrates the capacitor through the gaps in the package, which triggers the chemical reaction in the internal layers. The metal electrodes are transformed into poorly conductive hydroxides, and no electrical stress is required for the reaction to occur [13]. When the electrode material is the zinc alloy (Zn) or aluminum alloy (Al), the following reactions occur [8], [32]:

$$\begin{cases} \mathrm{Zn} + 2\mathrm{H_2O} \rightarrow \mathrm{Zn(OH)_2} + \mathrm{H_2} \\ 2\mathrm{Al} + 6\mathrm{H_2O} \rightarrow 2\mathrm{Al(OH)_3} + 3\mathrm{H_2} \end{cases} \tag{1}$$

where $\mathrm{Zn(OH)_2}$ and $\mathrm{Al(OH)_3}$ are metal hydroxides formed by humidity corrosion.

As shown in the partial film structure of the humidity corrosion in Fig. 2, the metallized layer is gradually corroded as a result of the chemical reactions described above. The dielectric film layer is mainly made of polypropylene, polyethylene, or other polymer materials, and is not subject to corrosion by humidity [17], [32].

The conductivity of the hydroxide is much worse than that of the metal alloy, resulting in a significant increase in the equivalent resistance of the metallization layer (e.g., r_{m_1} in the Fig. 2 of humidity corrosion part) [33]. Meanwhile, the reduction in electrode area leads to an equivalent open circuit (e.g., C_{d_1} in the humidity corrosion part) in the same dielectric film region, which is reflected in the reduction of the capacitance value. Existing studies have found that the degree of humidity corrosion is temperature dependent and increases as the temperature increases [13]. Meanwhile, the degree of humidity corrosion is closely related to the sealing degree of the capacitor. In general, high-power capacitors with great sealing are highly resistant to humidity corrosion. [34].

3) Electrochemical Corrosion: Aluminum or zinc alloy used in ac film capacitors have excellent capability to resist humidity corrosion, but exhibit weak stability due to electrochemical corrosion under high ac voltage stress [35]. Metallized film

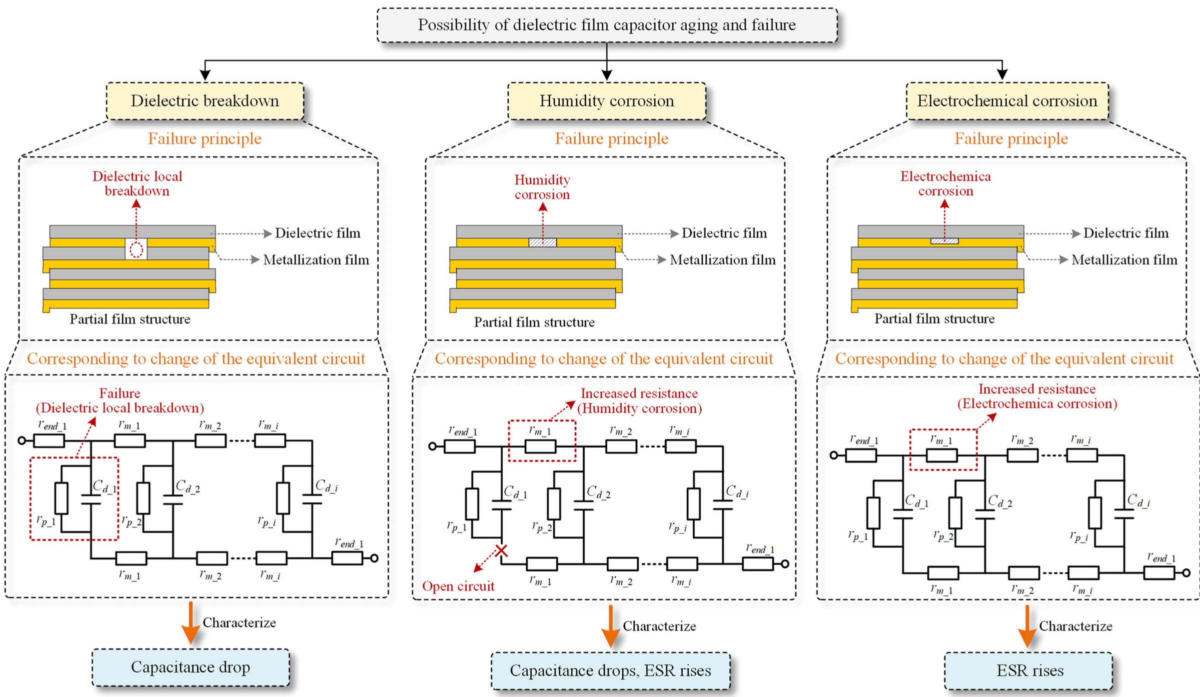

Fig. 2. Possibility of dielectric film capacitor aging and failure modes.

capacitors have a certain amount of interlayer air between the film layers. When the capacitors are used in ac applications, the metallized layer undergoes electrochemical corrosion with the following reactions [8], [16]:

$$\begin{cases} 2\mathrm{Zn} + \mathrm{O}_2 \rightarrow 2\mathrm{ZnO} \\ 4\mathrm{Al} + 3\mathrm{O}_2 \rightarrow 2\mathrm{Al}_2\mathrm{O}_3 \end{cases} \quad (2)$$

where ZnO and Al_2O_3 are metal oxides formed by electrochemical corrosion.

As shown in the partial film structure of the electrochemical corrosion part in Fig. 2, as the metal surface oxidation occurs, the products of electrochemical corrosion form a protective oxide film of ZnO, Al_2O_3, etc., can effectively prevent the metal from encountering atmospheric oxygen, thereby inhibiting further oxidation [16]. At this point for the dielectric film layer, there is still a certain thickness of metallized layer in contact with it.

The conductivity of the oxide is much worse than that of the metal alloy, resulting in a significant increase in the equivalent resistance of the metallization layer (as shown in r_{m_1} in the electrochemical corrosion part of Fig. 2). However, the oxide film formed prevents further contact between the metal and oxygen in the atmosphere. The dielectric film C_{d_1} corresponding to the equivalent resistance r_{m_1} of the metallization layer can still be connected at this time, and thus, the capacitance value does not change significantly [19], [21].

III. Experiments Configuration and Testing Results

A. *Test Configuration in Experiments*

Based on the above possible aging and failure modes for metallized film capacitors, the configuration of the accelerated aging test is designed. The theoretical schematic diagram is given in Fig. 3. The experimental platform consists of three main modules: the electrical stress generator, the capacitors under testing (CUTs) in the chamber, and the data acquisition (DAQ) system.

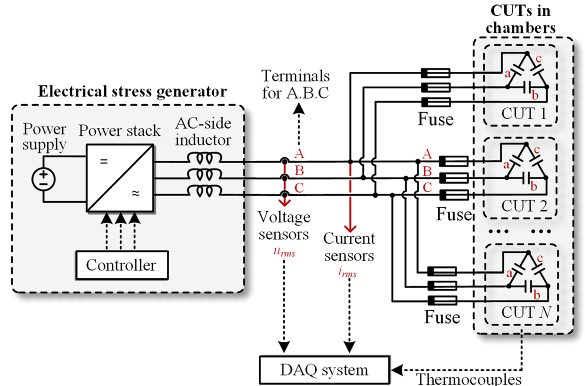

Fig. 3. Schematic diagram of the platform.

The electrical stress generator is used to provide ac voltage and ac current for CUTs, which adopts a recently reported method that has the advantage of a minimum required power supply and is robust to testing sample degradation [36], [37]. The ac current and ac voltage of the parallel connected CUTs are supplied by the electrical stress generator through the electrical terminal A, terminal B, and terminal C. When one of the CUTs is catastrophically failed it is replaced with a new one to keep the test of the other CUTs continuously. In this experimental platform, the three-phase line voltages u_{ab}, u_{bc}, and u_{ca} of

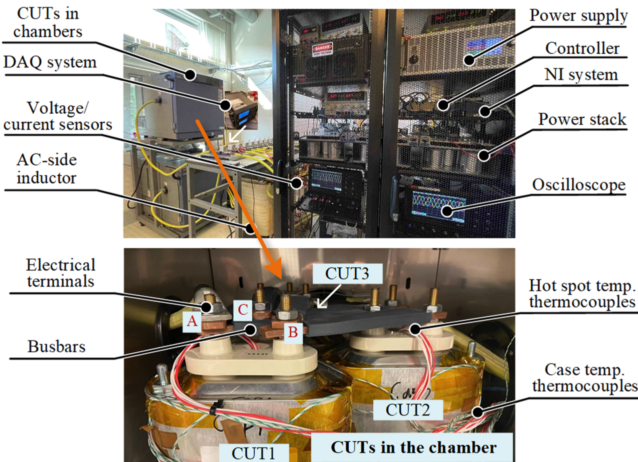

Fig. 4. Photo of the experimental platform. (a) Photo of stress emulation and DAQ equipment. (b) Photo of CUTs in the chamber.

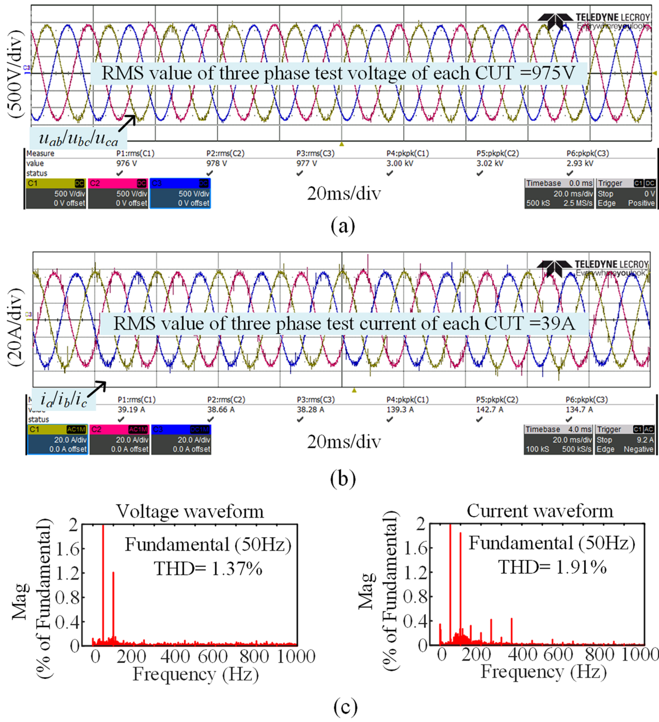

Fig. 5. Waveforms of test voltage and current for each CUT. (a) Voltage waveform for the each CUT. (b) Current waveform for the each CUT. (c) FFT analysis of voltage and current waveform.

TABLE II
SYSTEM AND CUTS PARAMETERS

Stress emulation setup	
DC power supply voltage U_{PS}	750 V
AC-side inductor L	2.5 mH
Switch frequency f_S	4000 Hz
CUTs setup for ac capacitors	
Capacitance of the CUT unit	75 μF
Rate ac voltage (rms) U_R	750 V
Testing ac voltage (rms) U_{rms}	975 V (1.3×U_R)
Rate ac current (rms) I_R	30 A
Testing ac current (rms) I_{rms}	39 A (1.3×I_R)
Testing frequency f_{test}	50 Hz
Testing ambient temperature	Case1: 87°C for CUT1 and CUT2 (Keep initial hot spot temperature at 100°C) Case2: 77°C for CUT3 and CUT4 (Keep initial hot spot temperature at 90°C)

the CUTs are acquired by the corresponding voltage sensors in three terminals. The three-phase phase currents i_a, i_b, and i_c of the CUTs are also acquired by current sensors. The CUTs are placed in the thermostat chambers to maintain a constant ambient temperature. The hot spot temperature can be obtained by burying the thermocouples at the core of the capacitor unit [in the middle of the mandrel as shown in Fig. 1(b)]. Meanwhile, thermocouples are installed in the cases of the CUTs to obtain the case temperature. The electrothermal stresses are collected in real time by DAQ systems [38] [39]. Based on this, the experimental platform is developed, as shown in Fig. 4.

The main stress emulation and CUTs setup parameters are given in Table II. In this testing, two cases are set up, setting the ambient temperature of the chamber to 87 °C and 77 °C, respectively. According to the safe operating voltage range in the datasheet and test standard for power capacitors, the testing ac current and ac voltage of each CUT is 1.3 times the rated value [40]. Fig. 5 shows the waveforms of ac voltage and ac current for each CUT. The fast Fourier transform (FFT) is done on the waveforms of voltage and current so that the fundamental and harmonic distributions of voltage and current at different frequencies can be obtained. Based on the calculation of the total harmonic distortion (THD) [41], the THD value is less than 2%, so the harmonic component can be neglected compared with the fundamental component. The rms value of ac voltage for each CUT is maintained at 975 V, where the rms value of ac current (equivalent current from terminal A, terminal B, and terminal C in Fig. 4) in the initial condition is 39 A.

B. Temperature Collection Results

The hot spot temperature of three capacitor units a, b, and c [shown in Figs. 1(a) and 4] in four CUTs are given in Fig. 6, the value of which is measured by the thermocouples and acquired in real time by the DAQ system. In these two cases, the initial hot spot temperature is 100 °C for CUT1 and CUT2 and 90 °C for CUT3 and CUT4. It can be seen that the hot spot temperature of CUTs gradually increases with the aging test time. There are certain differences in the failure times of CUT1 and CUT2, which may be due to sample tolerances for factory processes. It can be seen that the hot spot temperature increase trend is the same for CUT1 and CUT2 in Case 1. Similarly, the hot spot temperature rise trend is the same for CUT3 and CUT4 in Case 2. Comparing the test samples of Cases 1 and 2, the trend of temperature rise is different. This could be the effect of different ambient temperature settings. When the hot spot temperature of one capacitor unit of the CUTs reaches 140 °C or more, the possibility of CUTs catastrophic failure greatly increases. The temperature rises from hot spot to case of four CUTs are given in Fig. 7, respectively. From the results, the temperature rise of each capacitor unit averaged 13 °C at the initial testing and

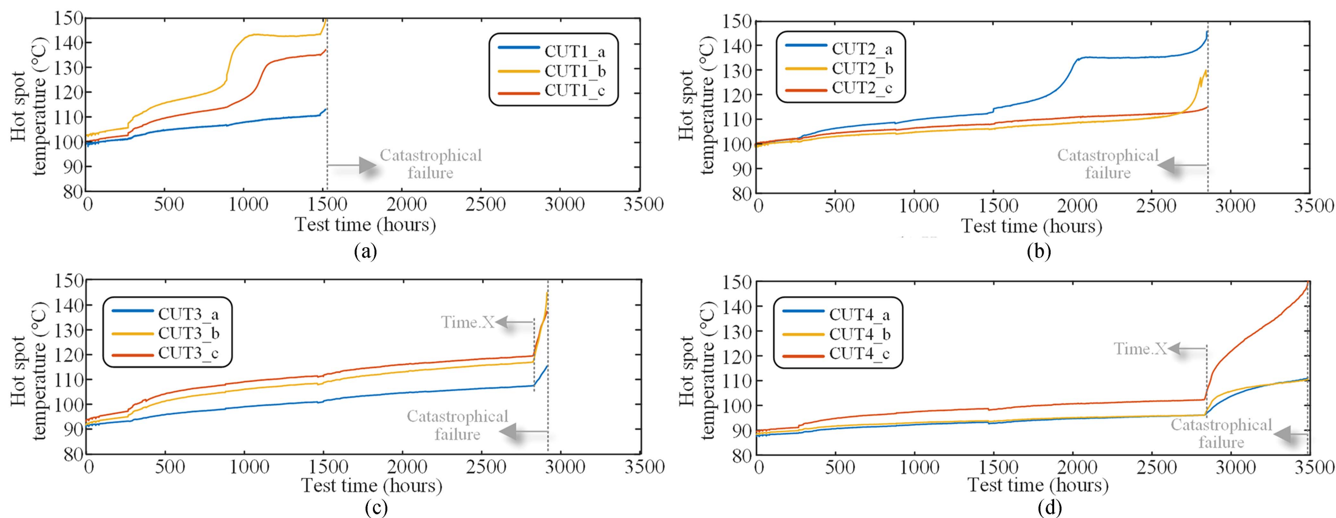

Fig. 6. Hot spot temperature for CUTs during aging degradation testing [collected by thermocouples in real time of Fig. 4(b)]. (a) Hot spot temperature of CUT1. (b) Hot spot temperature of CUT2. (c) Hot spot temperature of CUT3. (d) Hot spot temperature of CUT4.

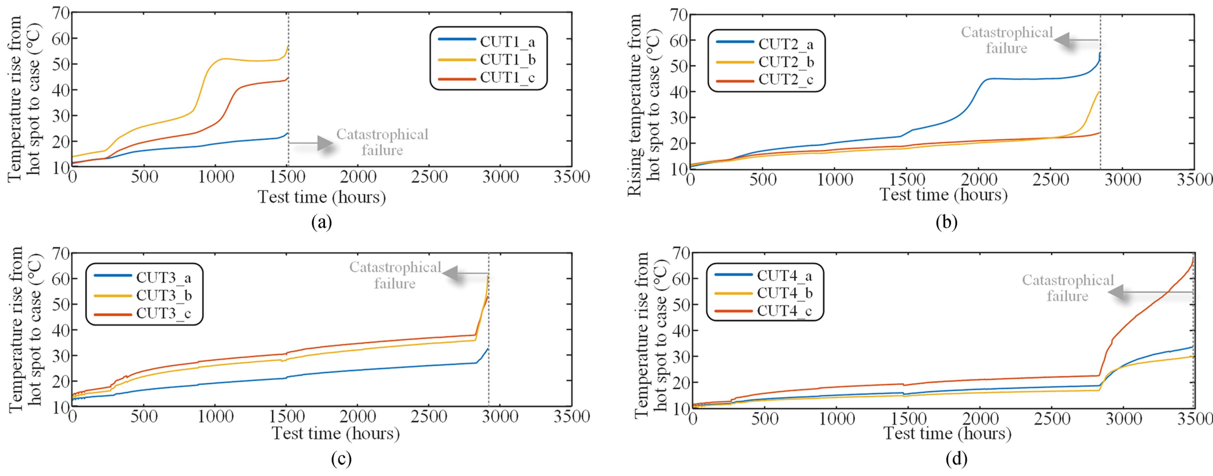

Fig. 7. Temperature rise from hot spots to cases for CUTs during aging degradation testing [collected by thermocouples in real time of Fig. 4(b)]. (a) Hot spot temperature and case temperature for CUT1. (b) Hot spot temperature and case temperature for CUT2. (c) Hot spot temperature and case temperature for CUT3. (d) Hot spot temperature and case temperature for CUT4.

gradually increased with the test time. When the temperature rise of one capacitor unit of the CUTs reaches 50 °C or more, the possibility of CUTs catastrophic failure greatly increases.

IV. Aging Indicators Extraction Based on Electrical–Thermal Analysis

A. Capacitance Extraction

The ac voltage U_{f_test} and ac current I_{f_test} of the CUTs at the specific frequency satisfy the following relationship:

$$\begin{aligned} U_{f_\text{test}} &= I_{f_\text{test}} \times Z_{\text{CUTs}} \\ &= I_{f_\text{test}} \times \left(\frac{1}{2\pi f_{\text{test}} C + \frac{1}{r_P}} + r_m + r_{\text{end}} \right) \end{aligned} \tag{3}$$

where Z_{CUTs} is the equivalent impedance of the CUTs, which is obtained by the equivalent electrical model in Fig. 1(b). f_{test} is the testing frequency of ac fundamental.

According to the equivalent parameters of the film capacitor, the insulation resistance typically falls within the megaohm level, while the ESR is typically in the milliohm range [28]. The relationship between r_m, r_{end}, C, and r_P at the specific testing frequency (50 Hz) is

$$\frac{1}{r_P} \ll r_m + r_{\text{end}} \ll 2\pi f_{\text{test}} C. \tag{4}$$

Therefore, ignoring the effects of the r_m, r_{end}, and r_p, the capacitance C of CUTs can be given as

$$C \approx \frac{I_{f_\text{test}}}{2\pi f_{\text{test}} \times U_{f_\text{test}}}. \tag{5}$$

The operating voltage and current in the accelerated aging testing are both 50 Hz sine waves, and the harmonic content is less than 2% in Fig. 5. Therefore, the capacitance value C can be calculated from the fundamental wave components of voltage and current at 50 Hz [42]

$$C = \frac{I_{f_\text{test}\,(50\,\text{Hz})}}{100\pi \times U_{f_\text{test}\,(50\,\text{Hz})}} \tag{6}$$

where $U_{f_\text{test}\,(50\,\text{Hz})}$ and $I_{f_\text{test}\,(50\,\text{Hz})}$ are the fundamental components of voltage and current extracted based on FFT at 50 Hz. The voltages and currents are acquired in real time by the DAQ system in Figs. 3 and 4.

It is worth noting that the change of C is affected by both temperature sensitivity and aging during the testing, in addition to operating voltage and current. The normalized capacitance with respect to its initial value along the testing time $K_{C(t)}$ can be expressed as

$$K_{C(t)} = K_{CT(t)} \times K_{CD(t)} \tag{7}$$

where $K_{CT(t)}$ and $K_{CD(t)}$ represent the normalized capacitance change caused by temperature sensitivity and aging during the testing, respectively.

B. Thermal Stress Parameters Extraction

The hot spot temperature T_{hot} [collected by thermocouples in real time of Fig. 4(b)] can be expressed as [5], [43]

$$T_{\text{hot}} = T_{\text{case}} + P_{\text{loss}} \times R_{\text{th}} \tag{8}$$

where T_{case} and R_{th} represent the case temperature of the CUTs and thermal resistance from hot spot to case, respectively. P_{loss} is the power loss of the CUTs.

According to the equivalent electrical model in Fig. 1(b), the power loss of CUTs is mainly caused by the loss generated by the electrical stresses on r_p and r_m [28], [44]

$$P_{\text{loss}} = I_{\text{rms}}^2 \times r_m + \frac{U_{\text{rms}}^2}{r_P} \tag{9}$$

where I_{rms} and U_{rms} represent the rms value of the testing ac current and ac voltage, respectively.

The temperature rise of CUTs from the case to the hot spot T_{rise} can be expressed as

$$\begin{cases} T_{\text{rise}} = T_{\text{hot}} - T_{\text{case}} = I_{\text{rms}}^2 \times r_{\text{Equ}} \times R_{\text{th}} \\ r_{\text{Equ}} = r_m + \dfrac{1}{4\pi^2 f_{\text{test}}^2 C^2 \times r_P} \end{cases} \tag{10}$$

where r_{Equ} represents the equivalent resistance of CUTs, and its value is affected by r_m, r_P, and C.

The change of r_{Equ} and R_{th} is affected by temperature sensitivity and aging during the testing, respectively. The normalized temperature rise with respect to its initial value $K_{r(t)}$ can be expressed as

$$K_{r(t)} = K_{rT(t)} \times K_{rD(t)} \tag{11}$$

where $K_{rT(t)}$ and $K_{rD(t)}$ represent the normalized change of temperature rise with temperature sensitivity and aging during the testing, respectively.

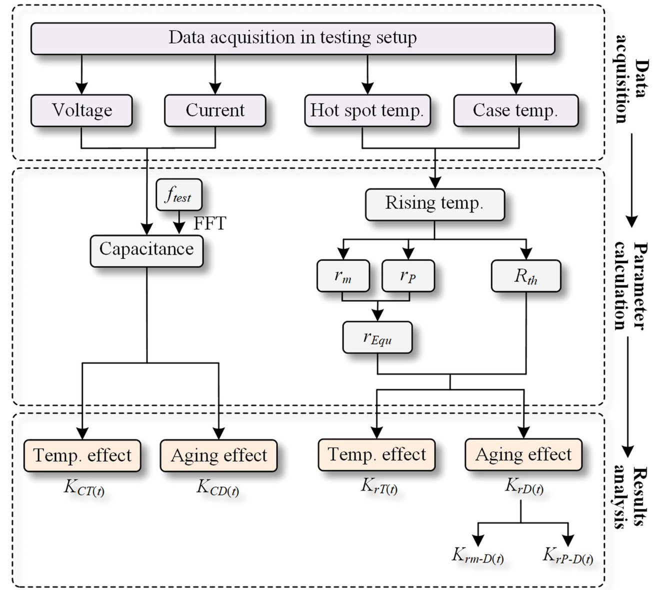

Fig. 8. Flowchart for aging and failure parameter analysis.

The change of $K_{rD(t)}$ is affected by both the ESR r_s and parallel insulation resistance r_P. Therefore, the normalized temperature rise change of CUTs with aging $K_{rD(t)}$ is given as

$$K_{rD(t)} = K_{rs-D(t)} \times K_{rP-D(t)} \tag{12}$$

where $K_{rs-D(t)}$ and $K_{rP-D(t)}$ represent the normalized change of ESR and parallel insulation resistance with aging during the testing, respectively.

C. Processes of Aging Indicators Extraction

Based on the above electrothermal stress analysis and modeling, the flowchart of the aging indicators can be obtained, which is divided into three steps: DAQ, parameters calculation, and results analysis, as shown in Fig. 8. First, the electrical stress signals of voltage and current, and the thermal stress signals of hot spot temperature and case temperature are collected in the data collection step. Next, the parameter calculation step is performed to obtain the capacitance and the temperature rise of the CUTs during the testing. Finally, the changes in capacitance, r_{Equ}, and R_{th} affected by temperature sensitivity and aging are quantified in the results analysis.

V. Failure Mechanism Analysis

A. Capacitance Results Analysis

Based on the collected ac voltage and ac current in the accelerated aging testing, the real-time capacitance results of the four CUTs can be derived according to (6), as shown in Fig. 9. This calculated capacitance represents the equivalent capacitance of the three terminal ac capacitors, which should be 1.5 times the capacitance of the individual capacitor unit given in Table II according to the structure of Fig. 1(a).

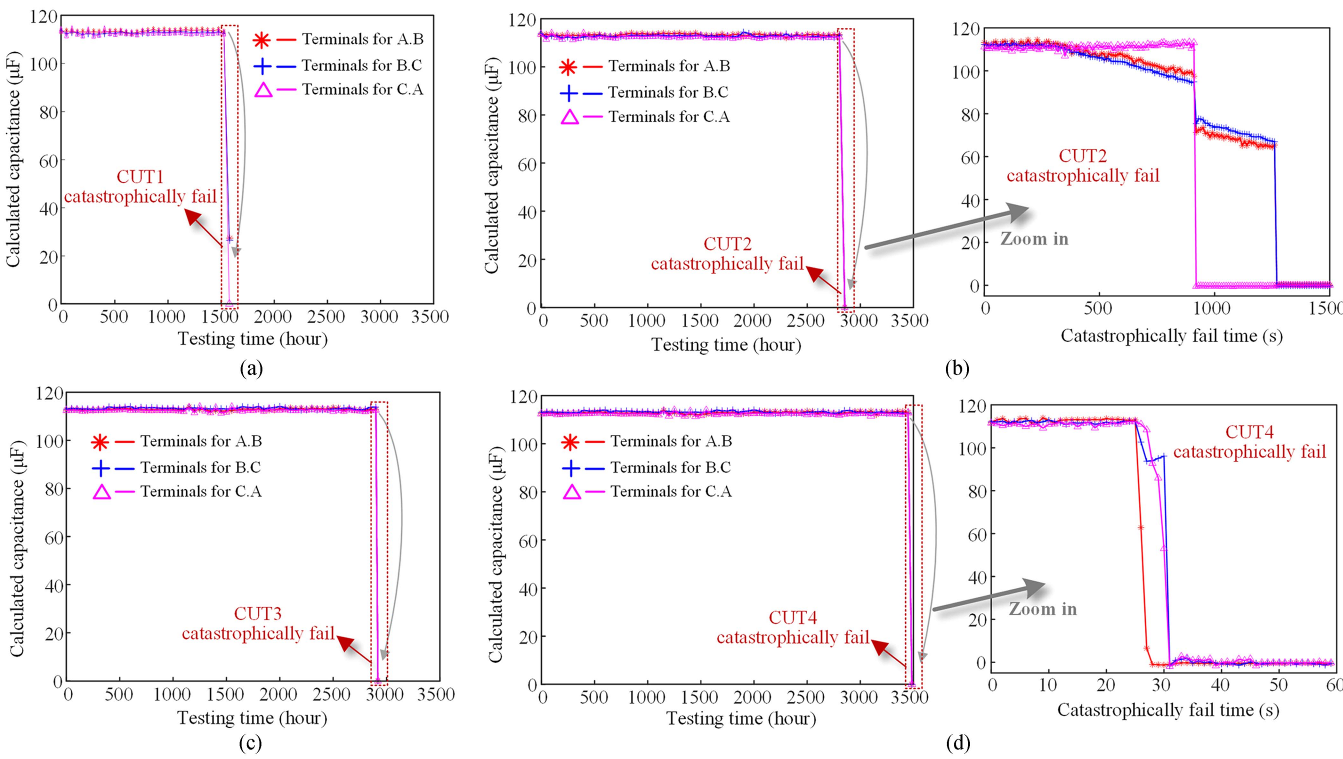

Fig. 9. Calculated capacitance for CUTs during aging degradation testing. (a) Calculated capacitance of CUT1. (b) Calculated capacitance of CUT2. (c) Calculated capacitance of CUT3. (d) Calculated capacitance of CUT4.

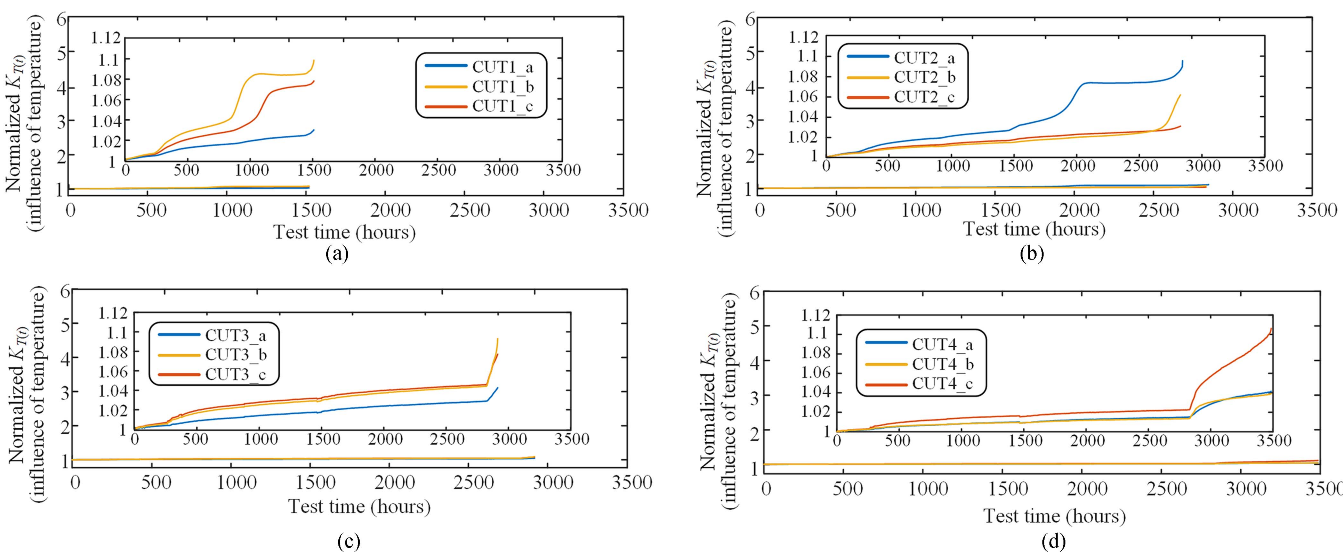

Fig. 10. Normalized $K_{T(t)}$ for CUTs (affected by the temperature, normalized temperature rise with respect to its initial value along the testing time). (a) Normalized $K_{T(t)}$ for CUT1 (influence of temperature). (b) Normalized $K_{T(t)}$ for CUT2 (influence of temperature). (c) Normalized $K_{T(t)}$ for CUT3 (influence of temperature). (d) Normalized $K_{T(t)}$ for CUT4 (influence of temperature).

The capacitance variation of the metallized film capacitor needs to consider the effect of temperature in (7). Fig. 19(a) in the Appendix shows the fitted curves of the corresponding capacitance at different temperature. It can be seen that the hot spot temperature of the CUTs rises from 90 °C to 140 °C from the time the CUTs start testing until they fail, encompassing a temperature-influenced capacitance change within 0.5%.

Therefore, it can be given that the capacitance of those four CUTs exhibits negligible reduction during the aging time before they fail. Zooming in on the results of the prefailure capacitance

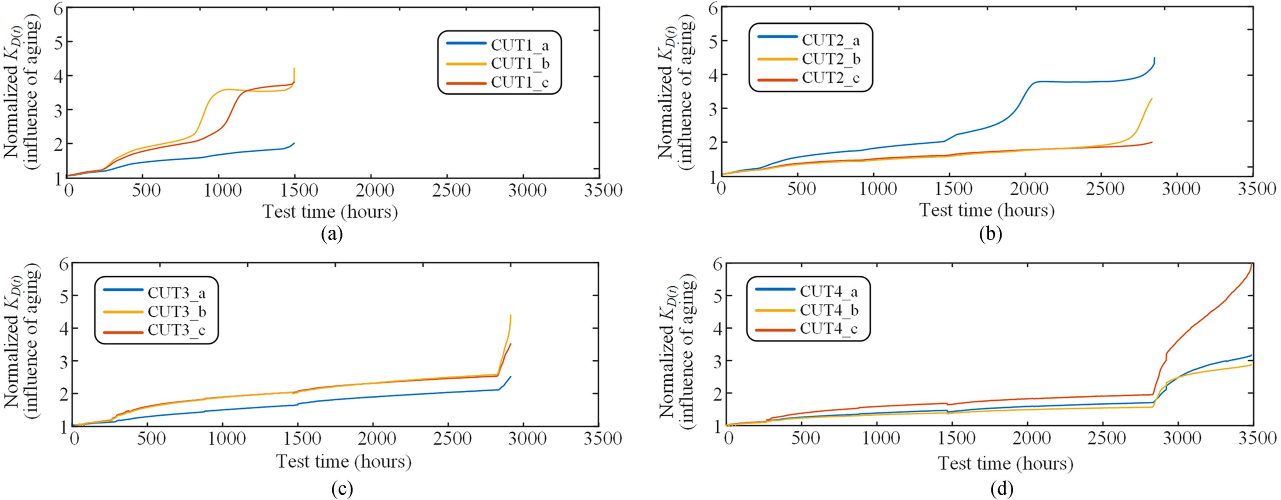

Fig. 11. Normalized $K_{D(t)}$ for CUTs (affected by the aging, normalized temperature rise with respect to its initial value along the testing time). (a) Normalized $K_{D(t)}$ for CUT1 (influence of aging). (b) Normalized $K_{D(t)}$ for CUT2 (influence of aging). (c) Normalized $K_{D(t)}$ for CUT3 (influence of aging). (d) Normalized $K_{D(t)}$ for CUT4 (influence of aging).

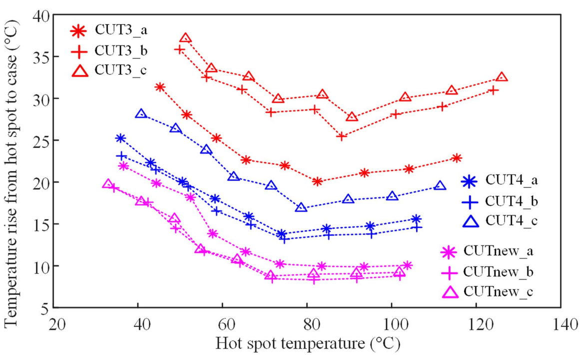

Fig. 12. Temperature rise of different CUTs at different temperatures. (CUT3 and CUT4 are tested at Time.X in Fig. 6).

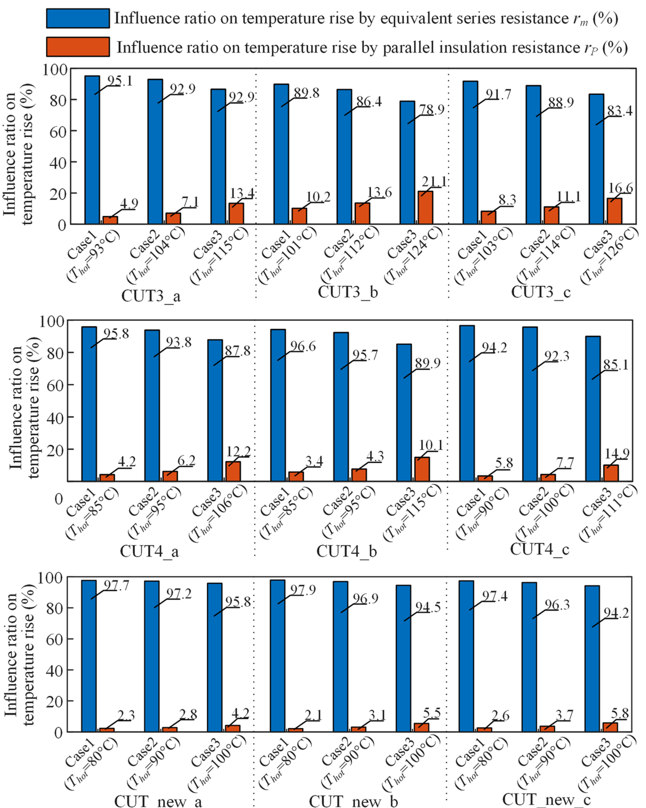

Fig. 13. Influence ratio on temperature rise by ESR r_m and parallel insulation resistance r_P with different hot spot temperature and different CUTs (Case1: testing ambient temperature = 70 °C, Case2: testing ambient temperature = 80 °C, and Case3: testing ambient temperature = 90 °C).

calculations, the capacitance of the CUT2 drops rapidly from the normal capacitance to zero in about 600 s before failure. Similarly, the capacitance of the CUT4 drops rapidly from the normal capacitance to zero in a short period (about 10 s) before failure.

B. Thermal Stress Results Analysis

Referring to (11), it is crucial to account for the impact of temperature sensitivity in evaluating the temperature rise variation of metallized film capacitors. In Fig. 19(b), fitted curves for r_s at different temperature are presented. The r_m of metallized film capacitors decreases as the temperature increases.

Furthermore, the thermal resistance (R_{th}) of polymers, such as polypropylene, decreases within the melting point range with increasing temperature [28], [45]. This initially leads to a decrease in the temperature rise of CUTs with the hot spot temperature increasing, as depicted in Fig. 20. When the applied ac current is constant, the change in temperature rise corresponds to the change in $r_{\text{Equ}} \times R_{\text{th}}$ according to (10). Subsequently, as the hot spot temperature continues to rise, the decrease in r_P causes an increase in the temperature rise of CUTs [28], [44]. By substituting the fitting curve into the testing results of temperature rise, the effect of temperature sensitivity on temperature rise can be eliminated.

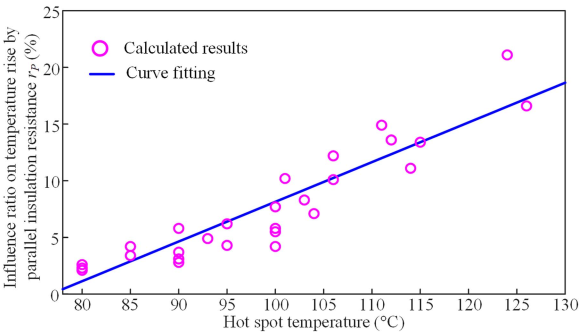

Fig. 14. Influence ratio on temperature rise by parallel insulation resistance r_P for different hot spot temperature.

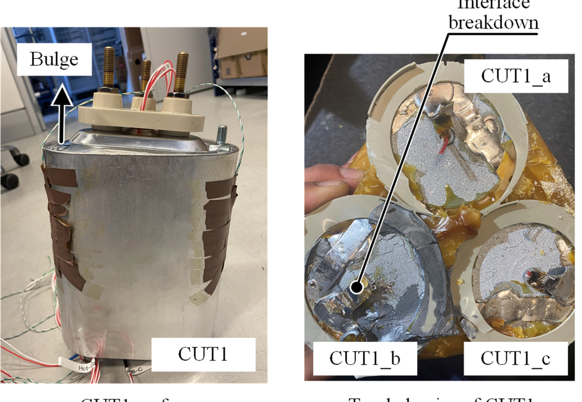

Fig. 15. Surface and behavior of catastrophically failed CUT1.

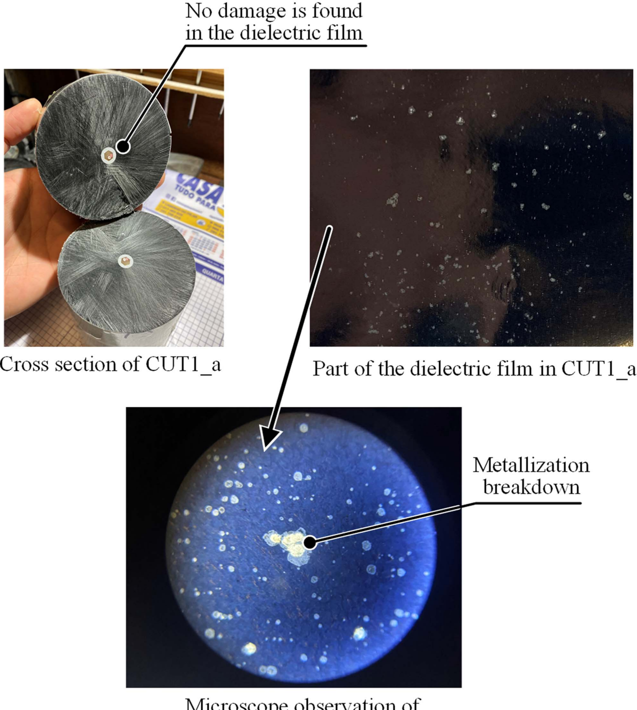

Fig. 16. Internal performance and microstructure evaluation of CUT1_a (one capacitor unit under degradation process, but not failed, as shown in Fig. 6).

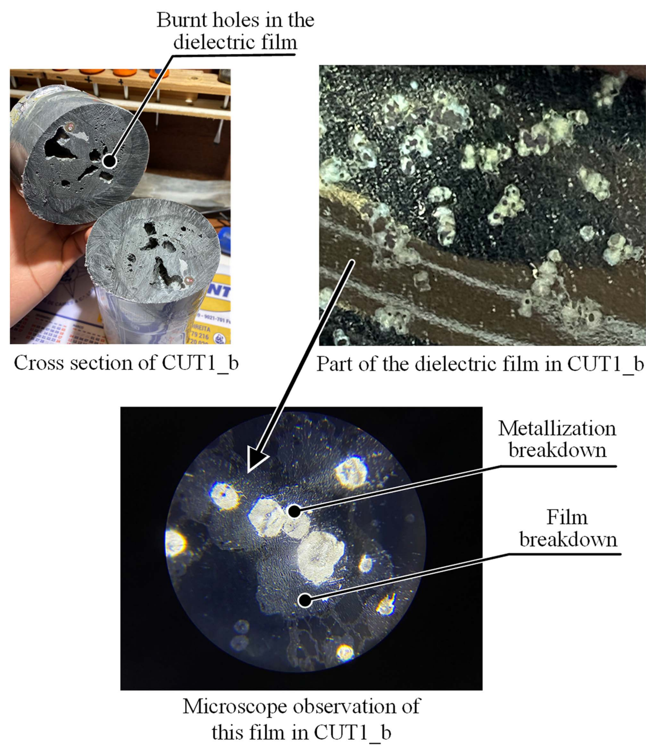

Fig. 17. Internal performance and microstructure evaluation of CUT1_b (one failed capacitor unit, as shown in Fig. 6).

Furthermore, the normalized temperature rises $K_{T(t)}$ with respect to its initial value along the testing time affected by temperature sensitivity can be obtained, respectively, as shown in Fig. 10. From the results, during the aging test time, the change of $K_{T(t)}$ with four CUTs affected by temperature sensitivity is less than 10%.

The metal electrode layer is of the order of nanometers and the polypropylene dielectric film layer is of the order of micrometers, so the thermal resistance internal to the film capacitor R_{th} is mainly generated by the dielectric film layer [18]. Since the dielectric film does not change significantly during the aging period (this conclusion is verified in the microscopic observations in the next section), the temperature rise caused by the aging of the capacitors can be considered to be mainly influenced by the equivalent resistance r_{Equ} in the metallization layer. After eliminating the effect of temperature sensitivity, the normalized temperature rises $K_{D(t)}$ affected by aging can be obtained, as shown in Fig. 11. When CUTs are failed, the $K_{D(t)}$ of CUT1_b, CUT2_a, CUT3_b, and CUT4_c are three times to five times increase, respectively. Comparing Figs. 10 and 11, the temperature rise for CUTs affected by aging is much greater than that by temperature sensitivity.

C. Series Resistance and Insulation Resistance Analysis

An increase in the equivalent resistance r_{Equ} can be characterized as a change in the ESR r_m and the parallel insulation resistance r_P. In the low-temperature stage (less than 70 °C),

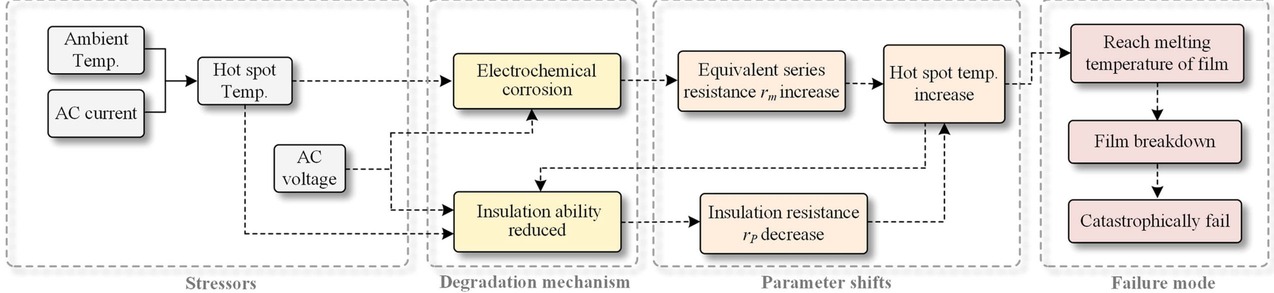

Fig. 18. Degradation and failure mechanism for AC filtering film capacitors.

the insulation resistance value r_m is generally greater than 10^5 M Ω, which can be ignored as an open circuit [45], [46]. According to the results in Fig. 20, it can be obtained that in the low-temperature stage (less than 70 °C), the temperature rise of the capacitor is mainly influenced by the R_{th} and the r_m. In addition, the insulation resistance of polypropylene capacitors decreases significantly with increasing temperature in the high-temperature stage (more than 70 °C) [28], [46]. Therefore, in the high-temperature stage, the effect of r_P on the temperature rise of the capacitor cannot be ignored.

The temperature rise of CUT3 and CUT4 corresponding to different hot spot temperatures are shown in Fig. 12. Depending on the different aging degrees of the CUTs, the temperature rise of CUT3 is higher than that of CUT4, and the temperature rise of CUT4 is higher than that of CUTnew. As the hot spot temperature increases, the temperature rise of the CUTs decreases and then increases. It can be considered that at low temperature, the increase in temperature rise (CUTnew → CUT4→CUT3) is mainly contributed by the increase of r_m. At the high temperature, the increase in temperature rise (CUTnew → CUT4→CUT3) is mainly contributed by the simultaneous increase of r_m and decrease of r_P.

Therefore, r_m can be calculated from the temperature rise of the low-temperature stage in Fig. 12 and the measured results of r_m in Fig. 19(b). Removing the temperature rise effect of r_m, r_P is calculated from the temperature rise of the high-temperature stage. The influence ratios on temperature rise by r_m and r_P for different CUTs are given in Fig. 13. As the hot spot temperature increases, the influence ratio of r_P on the temperature rise increases in each CUT unit. In addition, the greater the aging level of these three CUTs, the higher the influence ratio of r_P on the temperature rise.

Fig. 14 summarizes the influence ratio of r_P on the temperature rise corresponding to different hot spot temperatures with different CUTs. This influence ratio is linearly and positively related to the hot spot temperature. Therefore, with the CUTs aging, the r_m gradually increases, which causes the hot spot temperature to rise. When the hot spot temperature increases, the r_P gradually decreases, thus causing the hot spot temperature to rise significantly in the high-temperature stage.

VI. Microstructure Analysis and Failure Mechanisms

According to the results analyzed in the previous section, it is found that the capacitance is almost constant during the aging process, while the equivalent resistance is increasing. At the point of failure, the hot spot temperature reaches the melting point temperature of the polymer film and the capacitance decreases to zero (open circuit). Therefore, it is presumed that electrochemical corrosion possibly dominates the aging process, and the temperature rise caused by the increase of the equivalent resistance eventually leads to the failure of the CUTs. To verify this hypothesis, the section follows the physical and microscopic observations of the CUTs.

A. Microstructure Analysis

Fig. 15 illustrates the surface behavior of one CUT after failure. When the ac filter capacitors fail catastrophically, the top of the capacitors expands and bulges. Furthermore, the failed CUT1 is opened to observe the internal behavior of the ac capacitor. CUT1_a and CUT1_b are two capacitor units in the degradation process and catastrophic failure, respectively. Surface damage is observed on the top of CUT1_b after removal of the metal case.

The capacitor unit of CUT1 is cut, and the cross section of CUT1_a can be observed in Fig. 16. The metallization layer is of nanometer scale, and the dielectric film layer is of micron scale [18]. Since there is no obvious change in the cross section of CUT1_a, it can be assumed that the dielectric film of CUT1_a has not failed. A part of the film of CUT1_a is cut out, and the breakdown spots are found on the film of CUT1_a. By microscopic observation, the breakdown spots are caused by metallization breakdown, while no significant change is found in the dielectric film layer.

Similarly, the cross section of CUT1_b can be observed in the Fig. 17. Different from the CUT1_a, some holes are observed in the dielectric film of CUT1_b, which indicates that the dielectric film layer reached the melting point temperature (145 °C) [47]. Meanwhile, a few dense breakdown spots are found on the film of CUT1_b. The microscopic observation shows that there is not only the metallization breakdown but also the dielectric film breakdown in CUT1_b.

These behaviors indicate that during the degradation of the ac capacitor (such as CUT1_a in Fig. 16), the dielectric film does not break down, and thus, the capacitance has negligible reduction until the testing samples catastrophically fail. The metallization layer is gradually broken down locally during the degradation testing in Fig. 16, which increases its equivalent resistance, and its main occurrence is electrochemical corrosion.

The increase of the equivalent resistance further leads to the increase of the hot spot temperature. The possibility of capacitor catastrophic failure greatly increases when the hot spot temperature exceeds the melting point temperature of the dielectric film, as shown in Figs. 6 and 17.

B. Summary of Failure Mechanisms

Based on the analysis of the above test results and microstructure observation, a type of degradation and failure mechanism of ac filtering film capacitors can be summarized in Fig. 18. Under the long-term action of thermal stress and realistic ac voltage, the capacitors gradually undergo electrochemical corrosion. The metallization layer occurs oxidation, which increases its ESR r_m. The increase of r_m leads to a further increase in the hot spot temperature. When the hot spot temperature increases, the insulation ability of the capacitor reduces, and the r_P gradually decreases. It causes the hot spot temperature to rise significantly in the high-temperature stage. When the hot spot temperature exceeds the melting temperature of the polymer film, the dielectric film layer of the capacitor is broken down. The final result is a catastrophic failure of the ac filtering film capacitors.

VII. Conclusion

This article investigates the aging and failure mechanisms of a type of ac power filtering film capacitors used for MW power converters. Based on the analysis of about 3500 h of accelerated aging testing and the microstructure observations, a type of degradation and failure mechanism is summarized in Fig. 18. The analysis speculates that the electrochemical corrosion dominates the aging process and the following conclusions are obtained.

1) The capacitance has negligible reduction until the testing samples catastrophically fail under the specific testing conditions, which means that the capacitance is not suitable for a common precursor able to characterize degradation.
2) During the aging process, the metallization layer is gradually broken down, causing the hot spot temperature to rise. When the hot spot temperature rises to more than 140 °C, the possibility of capacitor failure greatly increases by the melting of the dielectric films.
3) With the capacitor aging, the ESR gradually increases, which causes the hot spot temperature to rise. The parallel insulation resistance decreases with the higher temperature, thus causing the hot spot temperature to rise significantly in the high-temperature stage.

The observations can provide a new perspective on the possible condition monitoring methods of film capacitors in ac filtering applications. For existing capacitance and ESR condition monitoring methods, it may be necessary to select ESR as a health indicator since the capacitance of this type of capacitor changes negligibly during aging. In addition, since the temperature rise of this type of capacitor is significant during aging and failure, the internally buried thermocouples or case temperature monitoring indicators have the potential for practical applications.

In the future, the authors will further develop their research in terms of application-oriented testing and micromaterial verification. 1) Performing aging testing at different frequencies to consider the effect of harmonics on aging and failure trends, and 2) considering microscopic material and chemical analyses of films in failed capacitors.

Appendix A
Offline Measurement of Capacitance and ESR

Offline measurement data and fitting curve of corresponding capacitance and r_m at different temperatures are given in Fig. 19. In Fig. 19(a), the capacitance is measured by two terminals of a new ac capacitor, which is used to eliminate the effect of temperature on capacitance in (7). In Fig. 19(b), the r_m is measured by a new single capacitor unit to avoid interference from terminal resistance and line resistance. The fitting curve of r_m is used to eliminate the effect of temperature on r_m in (11).

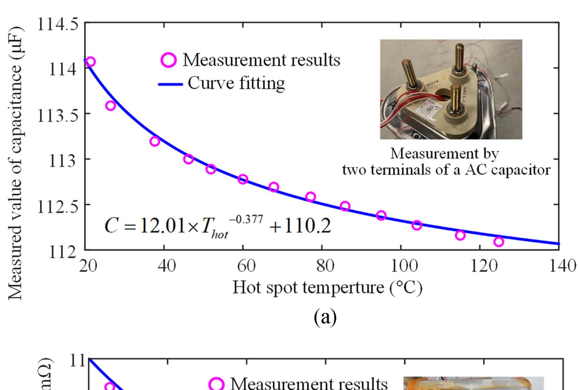

(a)

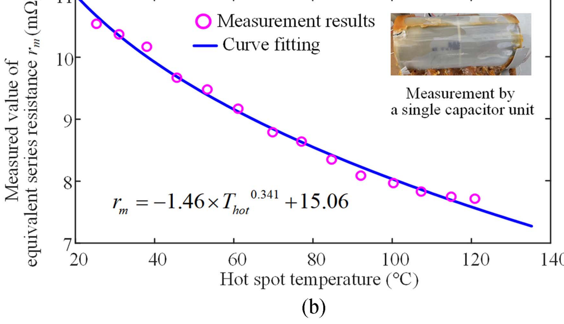

(b)

Fig. 19. Fitting curve of corresponding capacitance and r_m at different temperatures. (The data measured by Keysight LCR meter E4980a at 50 Hz, for eliminating the effect of temperature on capacitance and r_m). (a) Fitting curve of corresponding capacitance at different temperatures. (b) Fitting curve of corresponding capacitance r_m at different temperatures.

Fig. 20 shows the fitted curves of the testing results of corresponding temperature rise at different temperature conditions. The temperature rise of the CUTs decreases, and then, increases as the hot spot temperature increases when the applied ac current is constant in different temperature conditions.

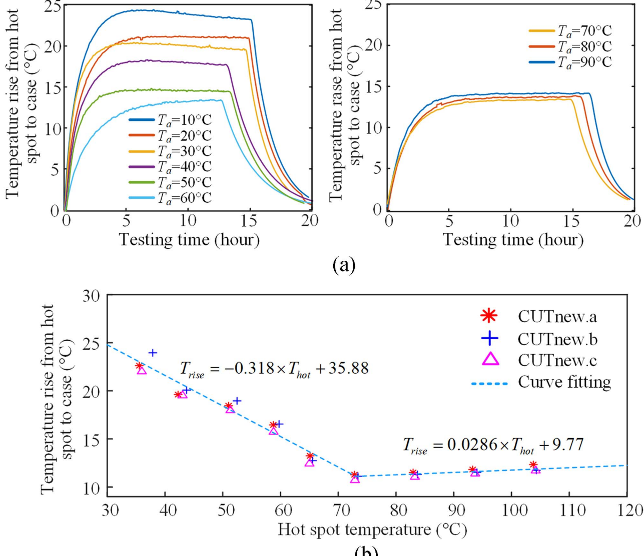

Fig. 20. Fitting curve of corresponding temperature rise for a new capacitor at different temperatures. (For eliminating the effect of temperature in (7), the CUTnew represents a new testing ac capacitor, and the result in (a) is the average temperature rise of the three units). (a) Temperature rise curve at different temperature. (b) Fitting curve of corresponding temperature rise at different temperatures.

References

[1] M. Bramoulle, “Electrolytic or film capacitors?” in *Proc. IEEE Ind. Appl. Conf.*, vol. 2, 1998, pp. 1138–1141.
[2] “Heavy duty three-phase AC filter capacitors,” *Electronicon*, 2018, [Online]. Available: https://www.powercapacitors.info/download/200.003-020051_E62-3ph.pdf
[3] D. Zhou, Y. Song, Y. Liu, and F. Blaabjerg, “Mission profile based reliability evaluation of capacitor banks in wind power converters,” *IEEE Trans. Power Electron.*, vol. 34, no. 5, pp. 4665–4677, May 2019.
[4] H. M. Umran, F. Wang, and Y. He, “Ageing: Causes and effects on the reliability of polypropylene film used for HVDC capacitor,” *IEEE Access*, vol. 8, pp. 40413–40430, 2020.
[5] H. Wang and F. Blaabjerg, “Reliability of capacitors for DC-link applications in power electronic converters-an overview,” *IEEE Trans. Ind. Appl.*, vol. 50, no. 5, pp. 3569–3578, Sep./Oct. 2014.
[6] B. Yao et al., “Electrothermal stress analysis and lifetime evaluation of dc-link capacitor banks in the railway traction drive system,” *IEEE J. Emerg. Sel. Topics Power Electron.*, vol. 9, no. 4, pp. 4269–4284, Aug. 2021.
[7] R. Gallay, “Metallized film capacitor lifetime evaluation and failure mode analysis,” in *Proc. CAS-CERN Accel. Sch. Power Converter*, 2015.
[8] N. Valentine, M. H. Azarian, and M. Pecht, “Metallized film capacitors used for EMI filtering: A reliability review,” *Microelectron. Rel.*, vol. 92, pp. 123–135, Jan. 2019. [Online]. Available: https://www.sciencedirect.com/science/article/pii/S0026271418310679
[9] W. Zhou et al., “Accelerated life testing method of metallized film capacitors for inverter applications,” *IEEE Trans. Transport. Electrific.*, vol. 7, no. 1, pp. 37–49, Mar. 2021.
[10] M. Makdessi, A. Sari, P. Venet, P. Bevilacqua, and C. Joubert, “Accelerated ageing of metallized film capacitors under high ripple currents combined with a DC voltage,” *IEEE Trans. Power Electron.*, vol. 30, no. 5, pp. 2435–2444, May 2015.
[11] M. Makdessi, A. Sari, and P. Venet, “Metallized polymer film capacitors ageing law based on capacitance degradation,” *Microelectron. Rel.*, vol. 54, no. 9-10, pp. 1823–1827, Jul. 2014.
[12] H. Li et al., “The capacitance loss mechanism of metallized film capacitor under pulsed discharge condition,” *IEEE Trans. Dielectr. Electr. Insul.*, vol. 18, no. 6, pp. 2089–2094, Dec. 2011.
[13] H. Wang, D. A. Nielsen, and F. Blaabjerg, “Degradation testing and failure analysis of DC film capacitors under high humidity conditions,” *Microelectron. Rel.*, vol. 55, no. 9-10, pp. 2007–2011, Aug./Sep. 2015.
[14] Y. Chen, H. Li, F. Lin, F. Lv, Z. Li, and M. Zhang, “Effect of interlayer air on performance of dry-type metalized film capacitor in DC, AC and pulsed applications,” *IEEE Trans. Dielectr. Electr. Insul.*, vol. 18, no. 4, pp. 1301–1306, Aug. 2011.
[15] C. Rochefort et al., “Ageing metallized polypropylene film capacitors laws confronted with the phenomenon of corrosion,” *Microelectron. Rel.*, vol. 150, Nov. 2023, Art. no. 115174.
[16] H. Li et al., “Capacitance loss mechanism and prediction based on electrochemical corrosion in metallized film capacitors,” *IEEE Trans. Dielectr. Electr. Insul.*, vol. 28, no. 2, pp. 654–662, Feb. 2021.
[17] H. Li, P. Lewin, and J. C. Fothergill, “Aging mechanisms of X2 metallized film capacitors in a high temperature and humidity environment,” in *Proc. IEEE Int. Conf. Dielectr.*, vol. 2, Apr. 2016, pp. 804–807.
[18] R. Brown, “Linking corrosion and catastrophic failure in low-power metallized polypropylene capacitors,” *IEEE Trans. Device Mater. Rel.*, vol. 6, no. 2, pp. 326–333, Jun. 2006.
[19] P. L. Lewin, J. C. Fothergill, and S. J. Dodd, “Electro-chemical degradation of thin film x2 safety capacitors,” in *Proc. IEEE Elect. Insul. Conf.*, 2015, pp. 98–101.
[20] J. Kirchhof and S. Kitterer, “Degradation from metallized polymer film capacitors with the dielectric polypropylene under the influence of humid heat,” in *Proc. Int. Exhib. Conf. Power Electron., Intell. Motion, Renew. Energy Manag.*, 2015, pp. 1–8.
[21] P. Mach and M. Horák, “Analysis of changes due to long-term thermal aging in capacitors manufactured from polypropylene film,” in *Proc. 43 rd Int. Spring Seminar Electron. Technol.*, 2020, pp. 1–5.
[22] D. F. Taylor, “On the mechanism of aluminum corrosion in metallized film ac capacitors,” *IEEE Trans. Dielectr. Electr. Insul.*, vol. DEI- 19, no. 4, pp. 288–293, Aug. 1984.
[23] “EMI suppression capacitors (MKP),” *TDK Electron. AG - EPCOS*, 2014, [Online]. Available: https://www.tdk-electronics.tdk.com/inf/20/20/ds/Y2_B32032_036.pdf
[24] ”Metallized polypropylene film capacitors (MKP),” *TDK Electron. AG - EPCOS*, 2019, [Online]. Available: https://www.tdk-electronics.tdk.com/inf/20/20/db/fc_2009/MKP_B32651_658.pdf
[25] “Heavy current capacitors,” VISHAY, 2017, [Online], Available: https://www.vishay.com/docs/13184/dischresisandcabcrosssect.pdf
[26] S. R. Swamy et al., “Metallized polypropylene film capacitors (MKP) dependent values with equivalent circuit,” 2014.
[27] H. Li et al., “Modeling of ESR in metallized film capacitors and its implication on pulse handling capability,” *Microelectron. Rel.*, vol. 55, no. 7, pp. 1046–1053, Jun. 2015.
[28] “General technical information: Film capacitors,” *TDK Electron. AG - EPCOS*, 2018. [Online]. Available: https://www.tdk-electronics.tdk.com/download/530754/480aeb04c789e45ef5bb9681513474ba/pdf-generaltechnicalinformation.pdf
[29] C. Lv et al., “A method to characterize the shrinking of safe operation area of metallized film capacitor considering electrothermal coupling and aging in power electronics applications,” *IEEE Trans. Ind. Electron.*, vol. 70, no. 2, pp. 1993–2002, Feb. 2023.
[30] M. Kong and Y. Lee, “Electrically induced heat dissipation in metallized film capacitors,” *IEEE Trans. Dielectr. Electr. Insul.*, vol. 11, no. 6, pp. 1007–1013, Dec. 2004.
[31] I. Rytöluoto, K. Lahti, M. Karttunen, and M. Koponen, “Large-area dielectric breakdown performance of polymer films - Part I: Measurement method evaluation and statistical considerations on area-dependence,” *IEEE Trans. Dielectr. Electr. Insul.*, vol. 22, no. 2, pp. 689–700, Apr. 2015.
[32] H. Li, T. Qiu, Z. Li, F. Lin, and Y. Wang, “Capacitance loss evolution of Zn–Al metallized film capacitors under atmospheric corrosion,” *IEEE Trans. Dielectr. Electr. Insul.*, vol. 29, no. 6, pp. 2363–2369, Dec. 2022.
[33] T. Qiu et al., “A proposed R-T model for atmospheric corrosion of metallized film in AC capacitors,” *IEEE Trans. Dielectr. Electr. Insul.*, vol. 29, no. 6, pp. 2258–2265, Dec. 2022.
[34] “Effect of humidity and condensation on power electronics systems in application note,” *Nat. Instruments*, 2022, [Online]. Available: https://www.semikron-danfoss.com/dl/service-support/downloads/download
[35] H. Li, T. Qiu, Z. Li, F. Lin, and Q. Zhang, “Analytical model for ionic current dominated corrosion of nanoelectrodes in metalized films: Frequency and electric stress,” *J. Chem. Phys.*, vol. 158, no. 11, , pp. 114702:1–8, Mar. 2023.
[36] B. Yao, Q. Wang, H. Wang, K. Hasegawa, and H. Wang, “A robust testing method for DC and AC capacitors with minimum required power supply,” *IEEE Trans. Power Electron.*, vol. 37, no. 5, pp. 4942–4946, May 2022.

[37] B. Yao, H. Wang, Q. Wang, and H. Wang, “A unified capacitor stress emulation method for high-power converter applications,” *IEEE Trans. Power Electron.*, vol. 38, no. 8, pp. 10213–10226, Aug. 2023.

[38] “CompactRIO Systems,” National Instruments, 2022, [Online]. Available: https://www.ni.com/da-dk/shop/compactrio.html

[39] “DAQ970 A data acquisition system,” *Keysight Technologies*, 2021, [Online]. Available: https://www.keysight.com/us/en/assets/7018-06259/technical-overviews/5992-3168.pdf

[40] ”Railway applications-rolling stock equipment-capacitors for power electronics,” Standard IEC 61881-1, 2011, [Online]. Available: https://webstore.iec.ch/publication/6058

[41] “Adjustable speed electrical power drive systems - part 2: General requirements - rating specifications for adjustable speed ac power drive systems,” Standard IEC 61800-2:2021, 2021. [Online]. Available: https://webstore.iec.ch/publication/62105

[42] K. Laadjal, M. Sahraoui, and A. J. M. Cardoso, “On-line fault diagnosis of DC-link electrolytic capacitors in boost converters using the stft technique,” *IEEE Trans. Power Electron.*, vol. 36, no. 6, pp. 6303–6312, Jun. 2021.

[43] B. Yao, X. Ge, H. Wang, H. Wang, D. Zhou, and B. Gou, “Multitimescale reliability evaluation of DC-link capacitor banks in metro traction drive system,” *IEEE Trans. Transport. Electrif.*, vol. 6, no. 1, pp. 213–227, Mar. 2020.

[44] S. Liu, Z. Shen, and H. Wang, “Safe operating area of DC-link film capacitors,” *IEEE Trans. Power Electron.*, vol. 36, no. 10, pp. 11014–11018, Oct. 2021.

[45] A. Dawson, M. Rides, and J. Nottay, “The effect of pressure on the thermal conductivity of polymer melts,” *Polym. Testing*, vol. 25, no. 2, pp. 268–275, Jan. 2006.

[46] “General technical information: Metalized film capacitors,” *Vishay Roederstein Company*, 2022, [Online]. Available: https://www.vishay.com/docs/26033/gentechinfofilm.pdf

[47] Y. He, F. Wang, J. Pan, H. M. Umran, L. Ran, and Z. Huang, “Effect of temperature on dielectric properties of metallized film capacitor,” in *Proc. Int. Conf. Electr. Mater. Power Equip.*, 2021, pp. 1–4.

Bo Yao (Graduate Student Member, IEEE) received the B.Eng. and M.Eng. degrees in electrical engineering from Southwest Jiaotong University, Chengdu, China, in 2017 and 2020, respectively, and the Ph.D. degree in power electronic from the Department of Energy, Aalborg University, Aalborg, Denmark, in 2023.

In 2023, he was a Visiting Scholar to the ABB Corporate Research Center, Vasteras, Sweden. He is currently in Postdoctoral Research with the Energy Department of Aalborg University. His research interests include reliability testing, and lifetime evaluation and condition monitoring of power electronic components in power converter systems.

Dr. Yao was the recipient of the Best Paper Award of *IEEE International Conference on Electrical Machines and Systems* in 2019, and the SEMIKRON Young Engineer Award from the European Center for Power Electronics and SEMIKRON Foundation in 2023.

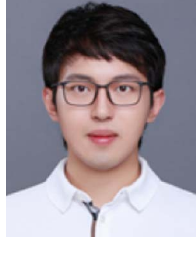

Xing Wei (Graduate Student Member, IEEE) received the B.E. degree in electrical engineering and automation from Nanjing Normal University, Nanjing, China, in 2016, and the M.E. degree in electrical engineering from Southeast University, Nanjing, in 2019. He is currently working toward the Ph.D. degree in power electronic with Aalborg University, Aalborg, Denmark.

From 2017 to 2018, he was a Visiting Student with RWTH Aachen University, Aachen, Germany. He is currently a Research Assistant with Southeast University, Nanjing. His research focuses on health and condition monitoring of traction inverters for electric vehicles.

Yichi Zhang (Graduate Student Member, IEEE) received the B.S. degree in electrical engineering from Shenyang Agricultural University, Shenyang, China, in 2017, and the M.S. degree in power electronics from Southwest Jiaotong University, Chengdu, China, in 2021. He is currently working toward the Ph.D. degree in power electronic with Aalborg University, Aalborg, Denmark.

His research interests include failure mechanism analysis, physics-informed lifetime modeling, and condition monitoring of semiconductor switches in power electronics.

Pedro Correia received the B.Eng. and M.Eng. degrees in electronics and telecommunication engineering from Universidade da Madeira, Funchal, Portugal, in 2014 and 2018, respectively.

He is currently a Power Electronics Assistant Lead Engineer with Vestas Wind Systems A/S, Aarhus, Denmark. His research interests include reliability of power semiconductors, capacitors, and power converters in renewable applications.

Rui Wu (Senior Member, IEEE) received the B.Sc. degree in electrical engineering from the Huazhong University of Science and Technology, Wuhan, China, in 2009, the M.Sc. degree in power electronics from the China Electric Power Research Institute, Beijing, China, in 2012, and the Ph.D. degree in power electronics from Aalborg University, Aalborg, Denmark, in 2015.

In 2012, he was an Electrical Engineer with the China Electric Power Research Institute. He is currently a Lead Power Electronics Engineer with Vestas Wind Systems A/S, Aarhus, Denmark. His research interests include reliability of power semiconductors, capacitors, and megawatts-level power converters in renewable applications.

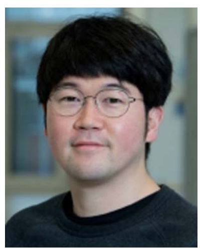

Sungyoung Song received the M.Sc. degree in electrical engineering from Changwon National University, Changwon, South Korea, in 2008, and the Ph.D. degree, thesis on reliability of GaN-on-Si high-electron-mobility transistors for power electronics application, from Aalborg University, Aalborg, Denmark, in 2018.

From 2008 to 2014, he was a Development Engineer of silicon-based semiconductor power devices with Magnachip Semiconductor Corp., Cheongju-si, South Korea. From 2019 to 2021, he was a Postdoctoral Fellow with the Department of Energy Technology, Aalborg University, where he worked on lithium-ion battery reliability for the Energy storage system application. Since 2022, he has been with Vestas Wind Systems A/S, Aarhus, Denmark, as a Lead Reliability Engineer. His research interests include reliability modeling, reliability test, lifetime evaluation, and condition monitoring of power electronic components in power converter systems.

Ionut Trintis (Member, IEEE) received the Dipl.Ing. degree in electrical engineering from the University Politehnica of Bucharest, Bucharest, Romania, in 2008, and the Ph.D. degree in power electronics from Aalborg University, Aalborg, Denmark, in 2012.

From 2012 to 2016, he was with the Department of Energy Technology, Aalborg University, working as Post Doc, Assistant Professor, and Associate Professor, teaching and working on research projects. From 2016 to 2022, he was with Vestas Wind Systems A/S designing multiple wind turbine power electronic converters. Since 2022, he has been with Siemens Gamesa Renewable Energy, designing offshore wind turbine power electronic converters. He has authored or coauthored more than 40 conference and journal papers, and he is the holder of three patents. His research interests include power electronics systems and components with focus on reliability, efficiency, and power density.

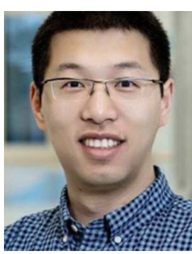

Haoran Wang (Member, IEEE) received the B.S and M.S. degrees in control science and engineering from the Wuhan University of Technology, Wuhan, China, in 2012 and 2015, respectively, and the Ph.D. degree in energy technology from the Center of Reliable Power Electronics, Aalborg University, Aalborg, Denmark, in 2018.

From 2013 to 2014, he was a Research Assistant with the Department of Electrical Engineering, Tsinghua University, Beijing, China. From 2017 to 2018, he was a Visiting Scientist with ETH Zurich, Zurich, Switzerland, and with Kiel University, Kiel, Germany, in 2019. From 2019 to 2021, he was an Assistant Professor with Aalborg University, Denmark, and Visiting Scientist with Vestas and Danfoss, Denmark. He is currently the Vice General Manager with Three Gorges Intelligent Industrial Control Technology Corporation Ltd., Wuhan, China. His research interests include reliability of electrical and electronic components and systems, multiobjective life-cycle performance optimization of power electronic systems, and reliable clean energy control systems.

Huai Wang (Senior Member, IEEE) received the B.E. degree in electrical engineering from the Huazhong University of Science and Technology, Wuhan, China, in 2007, and the Ph.D. degree in power electronics from the City University of Hong Kong, Hong Kong, in 2012.

In 2009, he was with the ABB Corporate Research Center, Switzerland. He was a Visiting Scientist with the Massachusetts Institute of Technology, Cambridge, MA, USA, from September to November 2013, and with ETH Zurich, Zurich, Switzerland, from August to September 2014. He is currently a Professor with AAU Energy, Aalborg University, Aalborg, Denmark, where he leads the group of reliability of power electronic converters and the mission on digital transformation and AI. His research interests include the fundamental challenges in modeling and validating power electronic component failure mechanisms and application issues in system-level predictability, condition monitoring, circuit architecture, and robustness design.

Dr. Wang was the recipient of the Richard M. Bass Outstanding Young Power Electronics Engineer Award from the IEEE Power Electronics Society in 2016 and the 1st Prize Paper Award from IEEE TRANSACTIONS ON POWER ELECTRONICS in 2021. He was an Associate Editor of *Journal of Emerging and Selected Topics in Power Electronics* and IEEE TRANSACTIONS ON POWER ELECTRONICS. He was elected as a Member of the Danish Academy of Technical Sciences in 2023.